ARAŞTIRMA MAKALESİ /**RESEARCH ARTICLE**

POLYMER-DERIVED SiOC CERAMICS; MORE QUESTIONS THAN ANSWERS

Hans-Joachim KLEEBE [1], Giuliano GREGORI [2]

ABSTRACT

Polymer derived SiOC ceramics (PDCs), with a rather high intrinsic carbon content, were characterized by transmission electron microscopy (TEM). One focus of this study was to highlight specific strengths as well as limitations of TEM specific techniques with high lateral resolution such as high-resolution TEM (HRTEM) and electron energy-loss spectroscopy (EELS). High-resolution TEM imaging revealed the predominantly amorphous nature of the bulk samples upon pyrolysis, while EELS analysis indicated the initiation of a phase separation process at temperatures exceeding 1000 °C. However, apart from valuable information that can be obtained by TEM studies with high lateral resolution, the question as to whether nanodomains form at elevated temperatures is still unsolved, in particular, since a phase separation of amorphous phases on the nanometer scale cannot easily be imaged by TEM. Therefore, Raman spectroscopy data are compared with HRTEM imaging results and the distribution and evolution of the intrinsic excess free carbon phase with increasing heat treatment temperature is critically discussed.

Keywords: Polymer-derived ceramics, SiOC, Transmission electron microscopy, Excess free carbon, Nanostructure, Raman spectroscopy.

POLİMERDEN TÜRETİLMİŞ SiOC SERAMİKLERİ; CEVAPLARDAN ÇOK SORULAR

ÖZ

Yüksek karbon içerikli polimerlerden türetilmiş SiOC seramikleri (PDCs) geçirimli elektron mikroskobu (TEM) ile karakterize edilmiştir. Bu çalışmanın bir amacı TEM'in yüksek-ayırma güçlü TEM (HRTEM) ve elektron enerji-kayıp spektroskopisi (EELS) gibi özel tekniklerinin güçlü yönlerini olduğu kadar sınırlamalarını da göstermektir. Yüksek-ayırma TEM görüntüleri piroliz sonrası yığınsal numunenin amorf yapısını açıkça gösterirken, EELS analizleri 1000 °C'nin üzerindeki sıcaklıklarda faz ayrışma sürecinin başlangıcını göstermiştir. Buna rağmen, yüksek yanal ayırma gücüyle TEM çalışmalarıyla elde edilebilen değerli bilgilerin dışında, yüksek sıcaklıklarda nanodomeinlerin olup olmadığı sorusu özellikle nanometre ölçekte amorf fazların faz ayrışımı TEM ile kolaylıkla görüntülenmediği için henüz çözülememiştir. Bu nedenle, Raman spektroskopi verileri HRTEM görüntü sonuçlarıyla karşılaştırılır ve artan ısıl işlem sıcaklığına bağlı olarak fazla serbest karbon fazın dağılımı ve değerlendirilmesi kritik olarak tartışılır.

Anahtar Kelimeler: Polimerlerden türetilmiş seramikler, SiOC, Geçirimli elektron mikroskobu, Fazla serbest karbon, Nanoyapı, Raman spektroskopisi.

---

[1]Technische Universität Darmstadt, Institute of Applied Geosciences, Schnittspahnstr. 9, D-64287 Darmstadt, Germany.
[2], Max Planck Institute for Solid State Research, Heisenbergstr. 1, D-70569 Stuttgart, Germany.
Author to whom correspondence should be addressed.
Email: kleebe@geo.tu-darmstadt.de

1. INTRODUCTION

Staring from the mid seventies (Verbeek and Winter, 1974; Yajima et al., 1976), polymer-derived ceramics has gained increasing interest thanks for their promising properties. Compared to conventional ceramic powder processing methods, the homogeneity of the polymer precursors on the atomic/molecular level, the applicability of well-established polymer processing techniques, and the low processing temperatures are highly desirable PDC properties. In particular, the interesting possibility to fabricate high-purity oxide and non-oxide ceramics, while starting from organometallic precursors with low viscosity such as polysiloxanes, polysilazanes, polycarbosilanes and polycarbosilazanes, determined the increased research activities in this area. Over the years, numerous studies on the synthesis of organometallic precursors, which yield bulk ceramic compounds upon pyrolysis, were reported (Vaahs et al., 1992; Mucalo et al., 1994; Riedel et al., 1995; Yu et al., 1995; Bill and Heimann, 1996).

Pyrolysis temperatures of 800 to 1000 °C promote the organic-inorganic transition and typically result in an amorphous network. Subsequent heat treatment at temperatures exceeding 1200 °C initiates local crystallization of the thermodynamically stable phases. Monthioux and Delverdier (1996) were first to report that the excess free carbon phase is first to nucleate followed by SiC formation. The latter compound forms via carbothermal reduction reaction. While nucleation within the binary Si-C system was reported to start at temperatures between 900 to 950 °C, crystallization within the ternary Si-O-C system was observed at 1200 °C.

It is important to note that, depending on the PDC system studied, markedly different onset temperatures for the occurrence of the excess carbon phase were observed; the overall trend follows the behavior of an increased number of constituents within the amorphous network. However, increasing the number of constituents within polymer-derived ceramics, in order to improve thermal stability against crystallization, is not the only governing parameter. Chemical composition, polymer architecture and, in particular, residual porosity within the amorphous matrix also affect the overall crystallization behavior of the amorphous bulk considerably.

Although only limited information concerning SiOC material properties are available in literature, the reported data clearly highlight the potential of SiOC for high-temperature applications, as compared to pure silica glass (Renlund et al., 1991; Soraru et al., 1996; Pantano et al., 1999). Most of the SiOC glasses studied were synthesized employing sol-gel processing. Upon heat-treatment at 1000 °C, SiOC matrices usually represent amorphous covalent solids with the presence of free carbon and/or residual hydrogen (Soraru et al., 1988; Pantano et al., 1999). Raising the annealing temperature to 1200 °C and above, local decomposition due to the escape of gaseous species (SiO and/or CO) is accompanied by the formation of nanosized SiC crystallites (Breval et al., 1994; Schiavon et al., 2002). This latter behavior was observed by TEM in SiOC samples, derived by pyrolysis of a polysiloxane precursor obtained via the sol-gel process (Kleebe et al., 2001). The sol-gel synthesis route enables the formation of precursors with different compositions, by simply mixing the starting alkoxides (e.g. $HSiO_3$ and CH_3SiHO_2 units) in different molar ratios (Soraru, 1994). It is easy to recognize that a high content of the CH_3SiHO_2 unit results in a high carbon content in the pyrolysed ceramic. In order to understand how the Si-O-C amorphous network is locally structured, one can start from the SiO_2 glass structure and substitute two divalent oxygen atoms by one tetravalent carbon atom. The composition of a stoichiometric SiOC, which consists only of Si-O and Si-C bonds, is given by $SiC_xO_{2(1-x)}$. In this way also some $C(Si)_4$ units are formed (as proven by NMR analysis as for example described in Kleebe et al. 2006), leading to a strengthened glass network due to locally higher bond density. Therefore, all properties related to the structure of the SiOC glass network, e.g., glass transition temperature, viscosity, elastic modulus and hardness increase with a higher amount of incorporated carbon (Hammond et al., 1993; Bodet et al., 1996; Rouxel et al., 1999).

Microstructure evolution can be monitored using different experimental techniques such as transmission electron microscopy (TEM) parallel to electron energy-loss spectroscopy (EELS); the latter allows for the determination of compositional changes with high lateral resolution. Similarly, a stoichiometric SiOC glass ($T^H/D^H = 2$), heat treated between 1000 and 1400 °C, was also characterized by TEM/EELS techniques (Kleebe et al. 2001). It was shown that a phase separation process, $SiC_xO_{2(1-x)} \Rightarrow xSiC+(1-x)SiO_2$, starts at about 1200 °C and results in the formation of nanosized SiC precipitates embedded in an amorphous SiO_2 matrix. It is assumed that, although the phase-separation process has progressed at this stage, the matrix still contains a minor fraction of incorporated

carbon, since crystallization of a pure SiO_2 phase was not observed. TEM and EELS analysis were similarly utilized to characterize the overall microstructure and, in particular, the crystallization behavior of two non-stoichiometric SiOC materials. As compared to the stoichiometric sample, the variation of the volume fraction of the two starting precursors, i.e., $T^H/D^H = 1$ and 9, yielded SiOC glasses enriched in either free carbon and or nanosized silicon precipitates (Turquat et al. 2001). The Si-rich SiOC matrix revealed pronounced growth of Si crystallites, when annealed at 1300 °C for 10 or 100 hours. The observed grain coarsening is consistent with the classical Ostwald ripening process of spherical particles within an amorphous matrix (Gregori et al., 2006). All TEM studies on ternary PDC systems, in particular on SiCN and SiOC, clearly indicated the metastable nature of these bulk glasses, since crystallization into thermodynamically stable phases occurs upon thermal treatment at temperatures exceeding the pyrolysis temperature.

The SiOC compositions characterized here, PHMS and PHMS+60%DVB, contain a much higher carbon content, as compared to stoichiometric or near stoichiometric SiOC materials mentioned above (sol-gel route), due to a novel synthesis approach described in detail in Kleebe et al. 2006. The focus of the study presented here is twofold: (i) the presentation of HRTEM imaging results in addition to EELS analysis and Raman spectroscopy and (ii) a critical discussion of the obtained data, in order to highlight specific strengths and limitations of the corresponding characterization techniques.

2. EXPERIMENTAL PROCEDURES

The polymer-derived ceramics investigated here were prepared starting from two polymer formulations (PHMS and PHMS+60%DVB) as described in detail elsewhere (Kleebe et al. 2006). Upon pyrolysis at 1000 °C, the ceramics underwent a second heat treatment at 1200 and 1450 °C.

Transmission electron microscopy (TEM) imaging and EELS analysis were performed on TEM-foils obtained from bulk SiOC samples that were prepared following standard ceramographic routines: cutting, ultrasonic drilling, dimpling, and Ar-ion thinning to perforation followed by light carbon coating to minimize charging under the incident electron beam.

Electron energy-loss spectroscopy (EELS) was employed to examine the local chemical compositions with high lateral resolution; the

silicon L-edge (Si-L) and the carbon K-edge (C-K) where considered, in order to follow the rearrangements occurring in the Si-based network as well as in the free carbon domains upon exposure to temperatures ranging from 1000 to 1450 °C. For this purpose, a transmission electron microscope, Philips CM200 FEG, operating at an acceleration voltage of 200 keV and interfaced to a Gatan Imaging Filter (GIF) model 678 was used.

As an integral characterization technique to study the evolution of carbon domains upon thermal anneal, Raman spectroscopy was performed using a System 1000 (Renishaw plc) microprobe employing an Ar-ion laser with a wavelength of 514.5 nm.

3. RESULTS AND DISCUSSION

3.1 Transmission Electron Microscopy

Samples of both formulations prepared via pyrolysis at 1000 °C exhibit entirely amorphous microstructures. Annealing at 1200 °C results in the formation of nano-domains of SiO_2 and SiC. Although this cannot be clearly confirmed by HRTEM imaging, the analysis of the intensity profiles of the electron diffraction patterns revealed the presence of a signal at about $3.9\ nm^{-1}$ (corresponding to characteristic planar spacing in SiC) and a broad shoulder in the range of $2\text{-}6\ nm^{-1}$ (typical of SiO_2). Similar features are detected in the DVB-containing sample of composition 2, as depicted in Fig. 1. In the latter material, however, additional signals attributed to graphitic domains are visible at 4.8 and $8.3\ nm^{-1}$. The broad shoulder at $2.9\ nm^{-1}$ might be assigned to two overlapping contributions due to the presence of silica ($2.6\ nm^{-1}$) and graphitic carbon ($3.0\ nm^{-1}$), respectively. The absence of discrete diffraction points suggests that these domains are still amorphous. HRTEM analysis corroborates this hypothesis, as in both formulations no crystalline features could be detected. Heat-treatment at 1450 °C induces further structural modifications in both systems. This is consistent with previous NMR results indicating an extensive molecular rearrangement of the amorphous Si-O-C network resulting in the formation of tetrahedral units of SiC_4 ("SiC phase") and SiO_4 ("SiO_2 phase") at the expense of mixed units.

In the PHMS system, both signals centered at about 2.6 and $3.9\ nm^{-1}$ show an intensity increase, which underlines a proceeding rearrangement process at higher temperature. Additional peaks at ~7.0 and $\sim7.5\ nm^{-1}$ were ob-

served and are assigned to SiC. The weak signal located at ~4.8 nm^{-1} is assigned in turn to graphitic carbon.

Although the PHMS sample annealed at 1450 °C maintains a predominantly amorphous character (Fig. 2), it exhibits the presence of few turbostratic carbon features (marked by the arrow) in addition to a small number of nanosized SiC crystallites, highlighted in the Fourier-filtered image (inset b), were observed. Hence, even upon thermal treatment at 1450 °C, the PHMS material is still predominantly amorphous and exhibited only a low volume fraction of turbostratic carbon and SiC precipitates. Similarly, the electron diffraction pattern (EDP) of the PHMS+DVB specimen annealed at 1450 °C allows for the assignment of the corresponding ring spacing to SiC (3.9, 7.0, and 7.5 nm^{-1}) and to graphite-like features (3.0, 4.8, and 8.3 nm^{-1}). At this stage, turbostratic carbon is formed and the signal corresponding to the spacing between graphene layers along the c-axis (3.0 nm^{-1}) is clearly visible. The comparison of the EDP of materials 1 and 2 upon exposure to 1450 °C reveals much stronger radial profile intensities for the PHMS+DVB sample. This suggests that the number of graphite-like and SiC precipitates present in the DVB-enriched composition might be considerably higher than in the PHMS sample. HRTEM imaging confirmed that thermal treatment at 1450 °C predominantly yields the formation of a high fraction of turbostratic carbon, homogeneously distributed over the entire sample, as shown in the HRTEM image of Fig. 3.

3.2 EELS Analysis – Carbon K-Edge

EELS was performed in order to investigate the changes occurring within the free carbon phase as a function of the different annealing treatments. Fig. 4 shows the carbon K-edge spectra acquired from both formulations after each thermal treatment. Upon pyrolysis at 1000 °C, the PHMS spectrum shows features characteristic of amorphous carbon. The π^* peak at 284 eV is characteristic due to a high number of sp^2-sites within the amorphous matrix. Heat-treatment at 1200 °C apparently does not affect the arrangement of the carbon atoms, whereas annealing at 1450 °C results in a significant modification of the near-edge fine structure of the carbon K-edge. The π^* signal is more intense compared to the other two spectra and the σ^* peak at 292 eV is more evident here. These are typical features one can observe in the near-edge structure of graphite-like carbon, which, for instance, is included in Fig. 4 as reference.

The π^*/σ^* intensity ratio, which provides a reliable evaluation of the sp^2/sp^3 bonding ratio, was used to examine the evolution of the carbon chemical bonds with increasing annealing temperatures. Upon exposure at 1450 °C, the π^*/σ^* ratio is 15% higher than right after pyrolysis, indicating a remarkable increase of sp^2-sites within the bulk. The DVB-containing specimens show a different evolution of the local carbon environment. After pyrolysis at 1000 °C, the PHMS+60%DVB system already exhibits distinct π^* and σ^* peaks. Little differences among the three spectra can be recognized within the energy-loss regime ranging between 295 and 305 eV. Remarkably, the increment of the π^*/σ^* intensity ratio in this sample is less pronounced (only 5%) than in the pure PHMS formulation. Since HRTEM analysis revealed a large amount of graphitic structures (sp^2-hybridised carbon) upon annealing at 1450 °C, we conclude that sp^2-carbon sites are present already upon pyrolysis at 1000 °C.

3.3 Raman Analysis

Raman spectroscopy was also used in order to investigate the evolution of the free carbon phase embedded in the SiCO matrix. Raman spectra of disordered graphite-like carbon exhibit two characteristic signals: (i) the D band at ~1350 cm^{-1} with A_{1g} symmetry corresponding to the breathing mode of aromatic rings and (ii) the G band centred between 1580 and 1600 cm^{-1} with E_{2g} symmetry generated by in-plane bond-stretching of sp^2 carbon pairs (Traßl et al. 2000).

This mode is active at all sp^2 sites but not necessarily observed at those arranged in a six-fold symmetry. As shown in Ferrari and Robertson 2000, position, width and intensity of the D and G modes can be used to establish how the disordered carbon phase is arranged. Specifically, the I(D)/I(G) intensity ratio enables the evaluation of the carbon-cluster size, according to Eq. (1):

$$\frac{I(D)}{I(G)} = C(\lambda)L_a^2 \qquad (1)$$

where L_a is the lateral size of the carbon domain along the sixfold ring plane. The value of the coefficient C depends on the wavelength λ of the laser used to probe the samples (here, C = 0.0055 $Å^{-2}$ and λ=514.5 nm were used, as in Traßl et al. 2000).
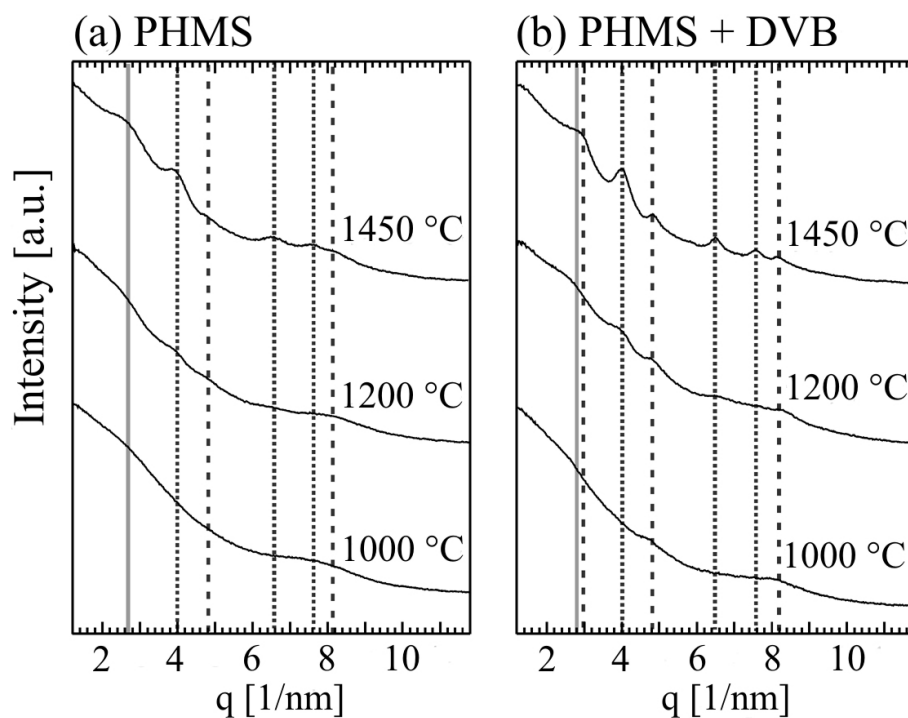
Fig. 1. Electron diffraction pattern profiles acquired from (a) PHMS and (b) PHMS + DVB. The evolution of the diffraction profiles with annealing temperatures indicate the progressive formation of SiO_2 and SiC domains along with graphitic carbon. The grey line corresponds to SiO_2, the dot-line to SiC and the dash-line to graphite like domain.
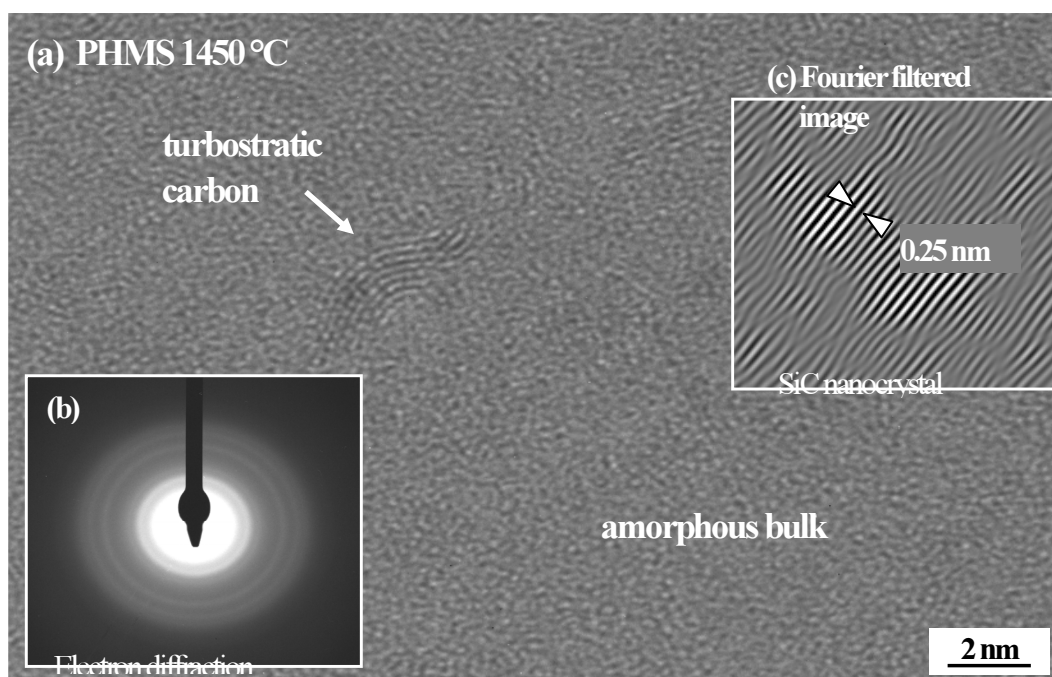

Fig. 2.(a) High-resolution TEM image of the PHMS sample heat-treated at 1450°C. Few isolated turbostratic carbon features can be recognized within the amorphous matrix as indicated by the arrow. (b) Corresponding diffraction pattern and (c) FFT-filtered images revealing the presence of SiC nanocrystals.
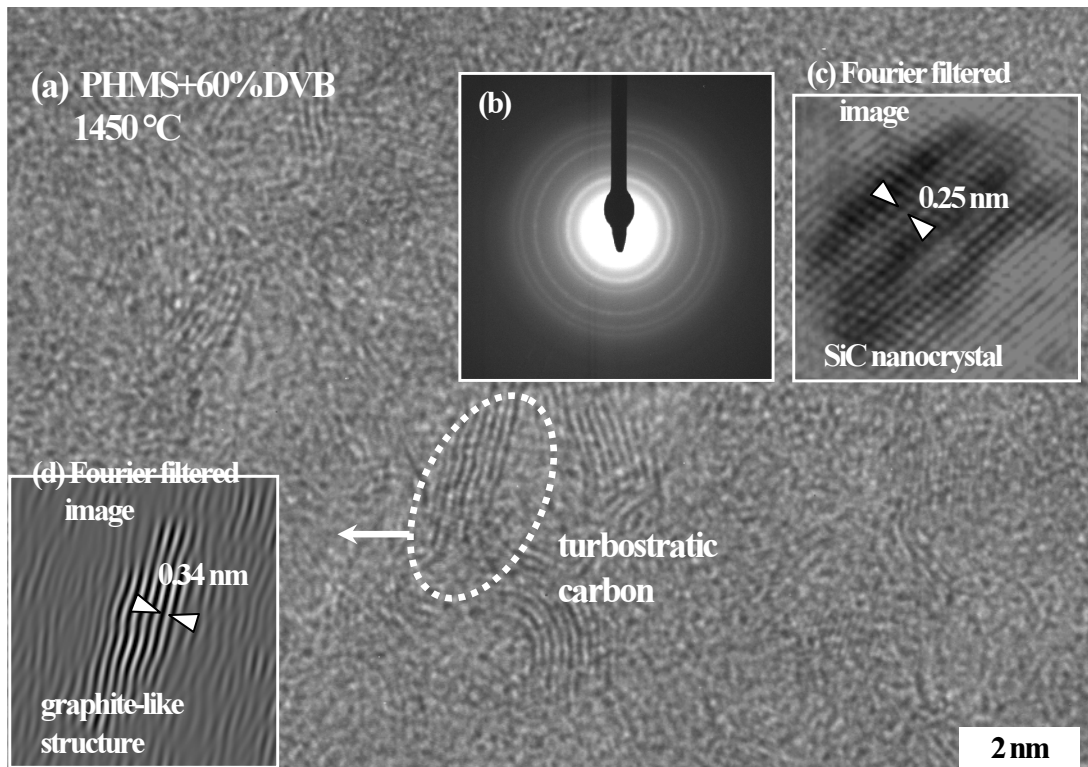
Fig. 3. (a) HRTEM micrograph of the PHMS + DVB sample exposed to 1450°C for one hour. Turbostratic carbon is present all over the bulk. (b) The corresponding EDP is characterized by a number of rings resulting from the presence of graphitic carbon and nano-scaled SiC crystallites. (c) FFT-filtered micrograph of turbostratic carbon. (d) FFT-filtered detail of a SiC nanocrystal.
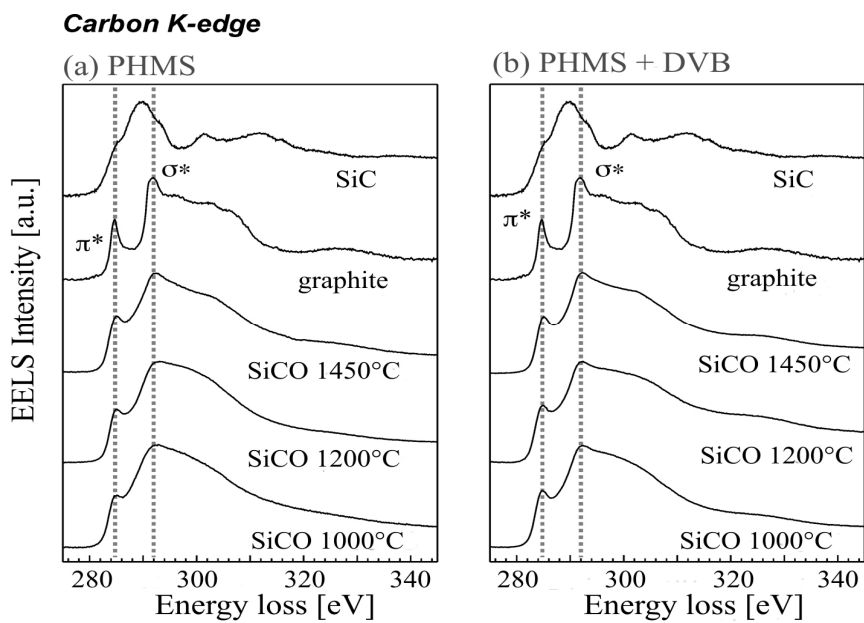

Fig. 4. Carbon K-edge EELS spectra of (a) PHMS and (b) PHMS + DVB. Energy loss spectra of SiC and graphite are shown for comparison. The dot-lines highlight the position of the π^* and σ^* peak at ~ 284 and 291 eV, respectively.

D and G bands obtained experimentally shown in Fig. 5 were fitted using Lorentzian curves, in order to calculate the I(D)/I(G) intensity ratios, which in turn allowed for the determination of L_a of all samples. For pure PHMS sample pyrolyzed at 1000 °C, the D and G peaks are rather noisy and broad, which is due to the pronounced structural disorder of the carbon phase. Spectra acquired from the samples annealed at 1200 °C exhibit very similar features. Apparently, this heat treatment does not modify the arrangement of the free carbon phase significantly. Conversely, data acquired from the specimen exposed to 1450 °C are characterized by very distinct and sharp D and G modes. This is consistent with an increasing sp^2/sp^3 bonding ratio (π^*/σ^* intensity ratio) observed during EELS analysis and suggests that an ordering process occurred within the predominantly amorphous SiOC ceramic network. Nevertheless, the lateral size L_a of the free carbon domains remains virtually unchanged (~1.6 nm) with increasing annealing temperature.

For the formulation with higher carbon content (PHMS+DVB), the spectra collected from these samples (Fig. 5) do not reveal a pronounced variation with increasing thermal treatment temperature. The corresponding I(D)/I(G) intensity ratio remained between 2.0 and 2.4, corresponding to a lateral cluster size of approximately 2.0 nm. The addition of DVB to the PHMS precursor and its cross-linking results in the formation of slightly larger graphitic clusters (likely graphene layers) already at 1000 °C. The excess amount of free carbon in material 2 is expected to result in a larger number of graphite-like carbon clusters but apparently it does lead to a larger domain size.

With respect to the excess of carbon in the DVB-containing PHMS composition, peak positions and intensities remain virtually unaffected by the different thermal treatments. This seems to suggest that neither a lateral growth nor a pronounced ordering process of the existing carbon domains occurs upon high-temperature annealing.

The experimental data presented above indicate that with increasing annealing temperature both SiCO compositions undergo a significant rearrangement of the amorphous network, which leads on the one hand to the formation of SiO$_2$ and SiC nanodomains and, on the other hand, to an increasing "graphitization" of the free carbon phase. Ultimately, SiC nanocrystals as well as turbostratic carbon can be clearly imaged by HRTEM upon exposure to 1450 °C.

3.4 Critical Data Assessment

Apart from the important implications which such a network evolution has on material properties, we would like to point out here capabilities and limitations of the experimental techniques used for the characterization of such amorphous networks.

As for the TEM analysis, electron diffraction patterns are extremely useful as they allow for the detection of the formation of nanodomains (SiO$_2$ vs. SiC) in the network particularly at lower temperatures (< 1200 °C). On the other hand, one should note that although high-resolution imaging has an excellent resolution limit (0.2 nm), it is extremely difficult to detect the local structural arrangement of amorphous materials. This is due to the fact that, although the resolution of modern TEM instruments is way superior to the variations in domain size discussed above, there is no constructive interference due to the short-range order typical of amorphous samples.

Hence, the HRTEM image, which is the Fourier back-transform of the electron diffraction pattern, cannot provide any detailed structural information of the amorphous solid, as commonly presented in high-resolution TEM micrographs of well-crystallized materials. This limitation persists as long as the domain size within the amorphous SiOC matrix is considerably smaller than the TEM sample thickness (approximately 1-2 nm versus 10-20 nm TEM-foil thickness).

Another intriguing aspect is represented by the lateral size La of graphitic carbon predicted by the analysis of the Raman results and the HRTEM images. Interestingly, the average dimension of the turbostratic carbon features detected by HRTEM exceeds La by about one order of magnitude, compared to 2.0 nm calculated by Eq. (1). This can be explained taking into account that the Raman results represent the average dimension of the graphitic lateral size, whereas the larger turbostratic features observed by HRTEM are simply easier to detect. It should be noted that turbostratic carbon can only easily be detected when the (0002) lattice planes are oriented perpendicular to the image plane (parallel to the incident electron beam).
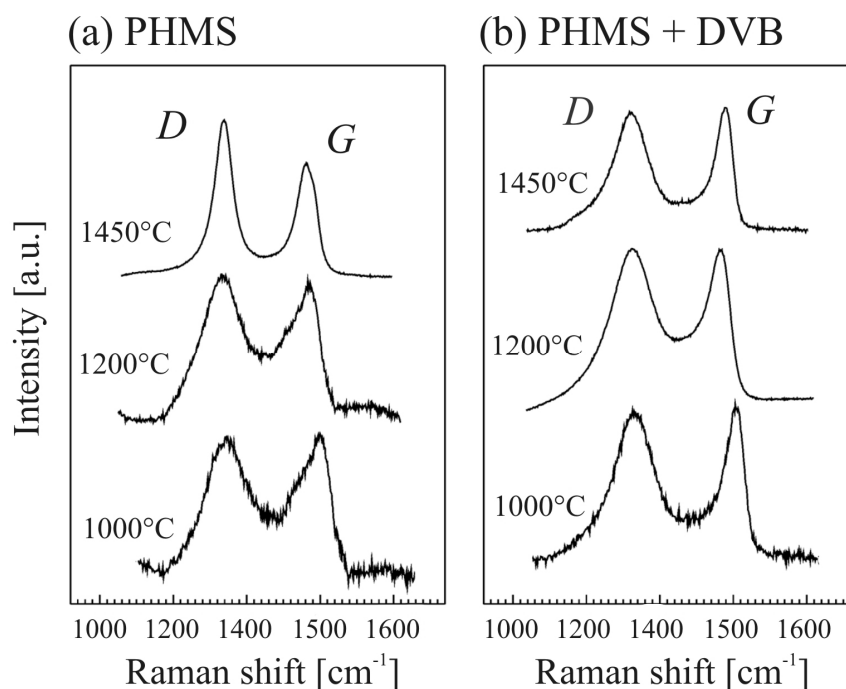
(a) PHMS

(b) PHMS + DVB

Fig. 5. Raman spectra acquired from (a) PHMS and (b) PHMS + DVB using a 514.5 nm green laser. The D and G bands characteristic of disordered graphitic carbon can be clearly recognized.

In addition, the number of layers constituting the turbostratic structure has to be large enough to allow for an unequivocal distinction by HRTEM. Consequently, due to electron optical restrictions, carbon clusters in low-temperature annealed matrices that are made of only one or two graphene-like layers are commonly not distinguishable from the surrounding amorphous SiOC network by HRTEM imaging.

Therefore, in the case of PHMS+60%DVB, one can reasonably assume that the sample upon pyrolysis at 1000 °C already contains a large number of well-dispersed, single or double-layered graphene planes, which however cannot be observed by HRTEM. This situation remains virtually unchanged up to an annealing temperature of 1200 °C, but undergoes a pronounced reconfiguration upon exposure to 1450 °C. Most likely, at this elevated temperature, graphene layers can grow or shift through the solid matrix and form multi-layered turbostratic carbon structures. Note that the transport mechanism of graphene layers through the SiOC matrix is unknown.

On the other hand, one should recognize that the Raman signal used for the determination of L_a arises from in plane vibrations. Indeed, the straight portions of the turbostratic carbon structures observed by HRTEM are consistent with the value of L_a of ~2.0 nm.

Hence, it is concluded that Raman analysis can only provide an estimation of the size of the straight portion of the graphene layers, which does not significantly change with higher annealing temperatures.

As for the SiC nanocrystals, their size is pretty much the same in both compositions. The main difference between the two samples consists merely in the number of SiC crystallites observed, which is surprising, considering the initial high aromatic content in the DVB-containing material. In the DVB-cured PHMS system, several SiC crystals were detected among the turbostratic carbon. It is worth to recall that, at this stage, the fraction of carbon atoms directly bonded to silicon, i.e., the carbon incorporated into the Si-based network, is higher in the DVB-containing formulation than in pure PHMS. Therefore, a higher fraction of SiC crystallites is expected. An interesting aspect, worth to discuss in this context, is where the Si-C bonds and therefore the SiC_4 units are most likely located within the amorphous bulk. Upon exposure to 1450 °C, carbon atoms in SiOC compounds can bond only to (i) other carbon atoms or (ii) silicon. In straight graphene layers, carbon atoms are all bonded to each other and do not have out-of-planes dangling bonds. Typically, these bonds are chemically very stable with the exception of atoms located at the edges. Therefore, it is assumed that most of the edges of the graphene layers are bonded to either Si (Si-C bonds) or oxygen

(C-O bonds, which are expected to be less stable at elevated temperatures). Note that HRTEM revealed the presence of SiC nanocrystals in close proximity to turbostratic carbon. However, in principle, the relatively high SiC content could also result from a local carbothermal reduction of silica ($SiO_2+3C \rightarrow SiC+2CO$), which typically occurs at temperatures exceeding 1300 °C. Here, the high carbon content, in particular of composition 2, could promote the carbothermal reduction reaction. However, thermo-gravimetric analysis of the carbon-rich sample revealed that carbothermal reduction is unexpectedly strongly suppressed in this system.

4. CONCLUSIONS

Various techniques were employed to investigate the nanostructure evolution of SiOC networks, depending on (i) their intrinsic carbon content and (ii) annealing temperature. This study has shown that HRTEM imaging of amorphous networks has its limitations, since, for example, it does not allow for the distinction of a local phase separation into SiO_2 and SiC domains. In addition, although Raman spectroscopy enables the detection of excess free carbon at an early stage of processing, i.e., upon pyrolysis, HRTEM does not reveal the presence of free carbon at low temperatures. In contrary, since Raman spectroscopy records in-plane vibration modes of carbon, the corresponding size distribution of carbon domains is underestimated (~one order of magnitude). Similar arguments can be used, when comparing HRTEM imaging or Raman spectroscopy with EELS analysis. Therefore, it is concluded that, in order to gain a consistent and representative 'picture' of a predominantly amorphous network, complementary techniques should be employed in parallel. The use of only one characterization tool will, most likely, generate a false 'image' and can easily lead to a misguiding interpretation of the intrinsic nanostructure.

ACKNOWLEDGEMENTS

REFERENCES

Bill, J. and Heimann, D. (1996). Polymer-Derived Ceramic Coatings on C/SiC-Composites. *J. Eur. Ceram. Soc.* 16, 1115-20.

Bodet, R., Jia, N. and Tressler, R.E. (1996). Microstructural Instability and the Resultant Strength of Si-C-O (Nicalon) and Si-N-C-O (HPZ) Fibres, *J. Eur. Ceram. Soc.* 16, 653.

Breval, E., Ammond, M. and Pantano, C.G. (1994). Nanostructural Characterization of Silicon Oxycarbide Glasses and Glass-Ceramics. *J. Am. Ceram. Soc.* 77 (11), 3012-3018.

Ferrari, A.C. and Robertson, J. (2000). Interpretation of Raman Spectra of Disordered and Amorphous Carbon. *Phys. Rev. B.* 61, (20) 14095-14107.

Gregori, G., Leebe, H.-J, Readey, D.W. (2006). Sorarù, G.D.; Energy-Filtered TEM Study of Ostwald Ripening of Si Nanocrystals in SiCO Glasses, *J. Am. Ceram. Soc.* 89 (5) 1699-1703.

Hammond, M., Breval, E, Pantano, C.G. (1993). Microstructure and Viscosity of Hot Pressed Silicon Oxycarbide Glasses. *Ceram. Eng. & Sci. Proc.* 14, 947-954.

Kleebe, H.-J., Turquat, C. and Sorarù, G.D. (2001). Phase Separation in a SiCO Glass Studied by Transmission Electron Microscopy and Electron Energy-Loss Spectroscopy. *J. Am. Ceram. Soc.* 84 (5), 1073-80.

Kleebe, H.-J., Gregori, G., Babonneau, F., Blum, Y.D., MacQueen, D.B., Masse, S. (2006). Evolution of C-rich SiOC Ceramics, Part-I. Characterization by Integral Spectroscopic Techniques: Solid-State NMR and Raman Spectroscopy, *Int. J. Mat. Res.* 97 (6), 699-709.

Monthioux, M. and Delverdier, O. (1996). Thermal Behavior of (Organosilicon) Polymer-Derived Ceramics, V: Main Facts and Trends. *J. Eur. Ceram. Soc.* 16, 721-37.

Mucalo, M.R., Milestone, N.B., Vickridge, I. C., Swain, M.V. (1994). Preparation of

Ceramic Coatings from Pre-Ceramic Precursors. *J. Mater Sci*. 29, 4487-99.

Pantano, C.G., Singh, A.K., Zhang, H. (1999). Silicon Carbide Glasses. *J. Sol-Gel Sci. and Technol*. 14,7-25.

Renlund, G.M., Prochazka, S., Doremus, R.H. (1991). Silicon Oxycarbide Glasses: Part I. Preparation and Chemistry and Part II. Structure and properties. *J. Mater. Res*. 6 (12) 2716-34.

Riedel, R., Kleebe, H.-J., Schönfelder, H., Aldinger, F. (1995). A Covalent Micro/Nano-Composite Resistant to High-Temperature Oxidation. *Nature*. 374, 526-28.

Rouxel, T., Massouras, G. and Sorarù, G.D. (1999). High Temperature Behavior of an SiOC Oxycarbide Glass: Elasticity and Viscosity. *J. Sol-Gel Sci. Technol*. 14, 83-94.

Schiavon, M.A., Soraru, G.D. and Yoshida, I.V.P. (2002). Synthesis of a Polysilazane Network and Its Evolution to Silicon Carbonitride Glass. *J. Non-Cryst. Solids*. 304, 76–83.

Sorarù, G.D. (1994). Silicon Oxycarbide Glasses from Gels. *Sol-Gel Science and Technology*. 2, 843-848.

Sorarù, G.D., Babonneau, F. and Mackenzie, J.D. (1988). Structural Concepts on New Amorphous Covalent Solids. *J. Non-Cryst. Solids*. 106, 256-261.

Sorarù, G.D., Dallapiccola, E. D'Andrea, G. (1996). Mechanical Characterization of Sol-Gel-derived Silicon Oxycarbide Glasses. *J. Am. Ceram. Soc*. 79, 2074-2080.

Traßl, S., Suttor, D., Motz G., Rössler, E. and Ziegler, G. (2000). Structural Characterisation of Silicon Carbonitride Ceramics Derived from Polymeric Precursors. *J. Eur. Ceram Soc*. 20, 215-25.

Turquat, C., Kleebe, H.-J., Gregori, G., Walter, S., Sorarù, G.D. (2001). TEM and EELS Study of Non-Stoichiometric SiCO Glasses. *J. Am. Ceram. Soc*. 84 (10), 2189-96.

Vaahs, T., Brück, M. and Böcker, W.D.G. (1992). Polymer-Derived Silicon Nitride and Silicon Carbonitride Fibers. *Adv. Mater*. 4 (3), 224-26.

Verbeek, W. and Winter, G. Shapes of Silicon Carbide and Methods for their Preparation. (in German), *German Pat. No*. 2236078 (1974).

Yajima, S., Okamura, K., Hayashi, J., Omori, M. (1976). Synthesis of Continuous SiC Fibers with High Tensile Strength. *J. Am. Ceram. Soc*. 59 (7-8), 324-27.

Yu, G., Ediringshe, M.J., Finch, D.S., Ralph, B., Parrick, J. (1995). Synthesis of α-Silicon Nitride Powder from a Polymeric Precursor. *J. Eur. Ceram. Soc*. 15, 581-590.